Computer Physics Communications 283 (2023) 108571

Contents lists available at ScienceDirect

Computer Physics Communications

www.elsevier.com/locate/cpc

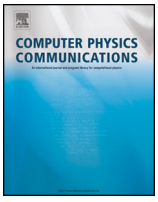

Automag: An automatic workflow software for calculating the ground magnetic state of a given structure and estimating its critical temperature ☆,☆☆

Michele Galasso [a,b,*], Artem R. Oganov [a]

[a] Skolkovo Institute of Science and Technology, Bolshoi Boulevard 30, bld. 1, 121205 Moscow, Russian Federation
[b] Lobachevsky State University of Nizhny Novgorod, Gagarin Avenue 23, bld. 2, 603022 Nizhny Novgorod, Russian Federation

ARTICLE INFO

Article history:
Received 24 August 2021
Received in revised form 19 October 2022
Accepted 21 October 2022
Available online 4 November 2022

Keywords:
Magnetic materials
Algorithm
DFT+U
Curie temperature
Néel temperature
Monte Carlo

ABSTRACT

We developed a Python package capable of finding the lowest-energy magnetic state of a given structure and to estimate its critical temperature from a Monte Carlo simulation of its effective Hamiltonian. In this paper, we introduce the code and present the results of tests performed on known materials: α-Fe_2O_3 (hematite), Ca_3MnCoO_6 and Ni_3TeO_6. After checking the calculation parameters for convergence, we computed the linear response value of U for DFT+U and then the single-point energies of a number of collinear magnetic configurations. The magnetic ground state has been correctly predicted for α-Fe_2O_3 and Ni_3TeO_6, while for Ca_3MnCoO_6 the DFT calculations did not reproduce the experimental low-spin states on Co atoms. For α-Fe_2O_3 and Ni_3TeO_6 we were able to estimate the Néel temperature and the computed values of 911 K and 31 K are both in good agreement with experiment (955 K and 52 K).

Program summary
Program title: Automag
CPC library link to program files: https://doi.org/10.17632/3b86n3rb8d.1
Developer's repository link: https://github.com/michelegalasso/automag
Licensing provisions: GNU General Public License 3
Programming language: Python3
Nature of problem: The first-principles study of the magnetic properties of a given material is a long and error-prone task, which is usually done by hand. Often scientists need to find the most stable magnetic state of a given structure, or at least its collinear approximation, and to get an estimate of the critical temperature of the magnetically ordered to paramagnetic phase transition.
Solution method: An automated search for the most stable magnetic state of a given structure and for the calculation of its critical temperature, which frees the users from repetitive work and keeps their attention on the physics of the problem. The code has a block structure which starts with convergence tests and ends with critical temperature calculation, allowing the users to skip anything that is not needed for their particular problem.

1. Introduction

The computational study of materials properties has become today more important than ever before. With the help of modern computers, scientists are now able to design new materials from scratch [1], something that was thought to be impossible just a few decades ago [2,3]. Moreover, the modern industry is in desperate need of new materials with optimal properties, e.g. superhard materials for the mining technologies, high-temperature superconductors for the energy and transport technologies and magnetic materials for the communication technologies. When a new material is designed and then discovered, the procedure followed is roughly the following: first a search for thermodynamically stable crystal structures is performed in a certain space of chemical compositions, then the physical properties of stable candidates are studied with accurate density functional theory (DFT) [4,5] calcu-

☆ The review of this paper was arranged by Prof. N.S. Scott.
☆☆ This paper and its associated computer program are available via the Computer Physics Communications homepage on ScienceDirect (http://www.sciencedirect.com/science/journal/00104655).
* Corresponding author at: Skolkovo Institute of Science and Technology, Bolshoi Boulevard 30, bld. 1, 121205 Moscow, Russian Federation.
E-mail address: michele.galasso@skoltech.ru (M. Galasso).

https://doi.org/10.1016/j.cpc.2022.108571
0010-4655/

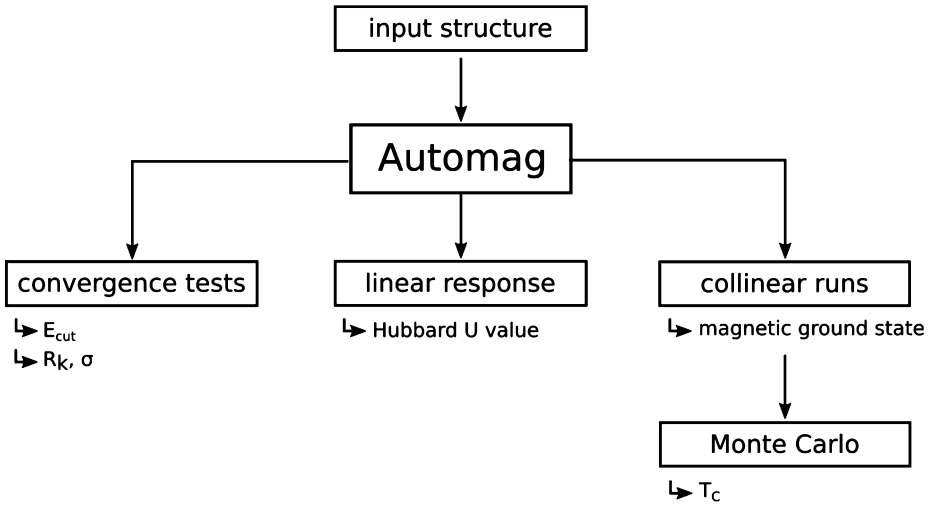

Fig. 1. Bird view of the Automag workflow. Four calculation steps form three independent paths: the first for convergence tests, the second for the calculation of the electronic correlation parameter U by linear response and the third for collinear magnetic calculations, which can be followed by an estimation of the critical temperature.

lations, and finally, if a new material with some desirable property is predicted, scientists attempt its experimental synthesis.

During the last decades, several algorithms have been proposed for solving the crystal structure prediction problem, among which we mention evolutionary algorithms [6–9] and the USPEX code [10–12], metadynamics [13,14], minima hopping [15], particle swarm optimization [16], random sampling [17,18] and simulated annealing [19,20]. However, when a number of low-energy structures are spotted using one of the above-mentioned methods, the detailed investigation of their physical properties is often still done by hand.

This work focuses on magnetic materials and it introduces Automag, a workflow software which automates the search for the ground collinear magnetic state of a given structure and the calculation of its critical temperature. In our method, we perform single-point energy calculations at the generalized gradient approximation level [21] of DFT using the projector-augmented wave method [22] as implemented in the Vienna Ab initio Simulation Package (VASP) code [23–25]. For handling VASP calculations efficiently, we use the FireWorks [26] library combined with a MongoDB remote database, while for estimating the critical temperature of the magnetically ordered to paramagnetic phase transition we use the VAMPIRE [27] software package. A workflow similar to Automag has been recently proposed [28] as part of the atomate code [29], which uses pymatgen [30] to generate a number of collinear magnetic configurations of a given structure. The configurations are then relaxed using DFT in order to determine which is the ground magnetic state. Automag constitutes a step forward with respect to this work because:

1. it does not use pymatgen for generating magnetic configurations (which can get stuck because of combinatorial explosions), but it directly communicates with the lower-level library enumlib [31,32];
2. it allows the user to automatically perform convergence tests and to calculate the linear response value of U [33] for the DFT+U formalism [34–36], without relying on Materials Project [37] parameters;
3. it can estimate the critical temperature of the magnetically ordered to paramagnetic phase transition.

Section 2 illustrates the algorithm and presents the Automag code, written with the purpose of automating long, repetitive and error-prone tasks and letting the user focus on the physical meaning of the results. Section 3 presents the results of tests performed on three materials: α-Fe_2O_3 (hematite) [38], Ca_3MnCoO_6 [39] and Ni_3TeO_6 [40], which are all well-known collinear antiferromagnetic systems. Finally, section 4 contains conclusions and ideas for future developments. The Automag code is available on GitHub,[1] and it is distributed under the GNU General Public License.

2. Overview of the algorithm

The Automag workflow is summarized in Fig. 1. It consists of four calculation steps arranged along three independent paths. The first two steps, "convergence tests" and "linear response" are completely independent and they automate the preparatory work that the user may need to perform before searching for the ground magnetic state of a given structure. The other two form a single path, meaning that the results of the "collinear runs" are needed as input to the "Monte Carlo" step.

The first step of the Automag workflow automates the convergence tests for the VASP parameters E_{cut}, σ, and R_k which are, respectively, the energy cut-off of the plane wave basis set, the electronic smearing parameter and the k-mesh resolution parameter for Brillouin zone sampling. The parameter R_k is used by VASP for determining the number of subdivisions N_i along the reciprocal lattice vectors b_i for the automatic generation of a Γ-centered Monkhorst-Pack grid according to eq. (1).

$$N_i = \mathrm{int}(\max(1, R_k * |\vec{b_i}| + 0.5)) \quad (1)$$

Since the parameters R_k and σ are very much interdependent, their convergence is checked simultaneously.

The second step automates the calculation of the electronic correlation parameter U by linear response. Strongly correlated materials, such as transition metal oxides, are poorly described by DFT and can be better studied using the DFT+U formalism. The linear response approach is a very convenient way of calculating the value of U, since its fit based on experimental data is often not possible during theoretical materials design. For DFT+U, we use the simplified approach of Dudarev et al. [41].

The third step generates a number of collinear ferromagnetic (FM), antiferromagnetic (AFM) and ferrimagnetic (FiM) configurations and then uses VASP to compute their single-point energy, in order to find out which is the most thermodynamically stable. A completely non-magnetic (NM) configuration is also generated.

[1] `Automag` codebase: https://github.com/michelegalasso/automag.

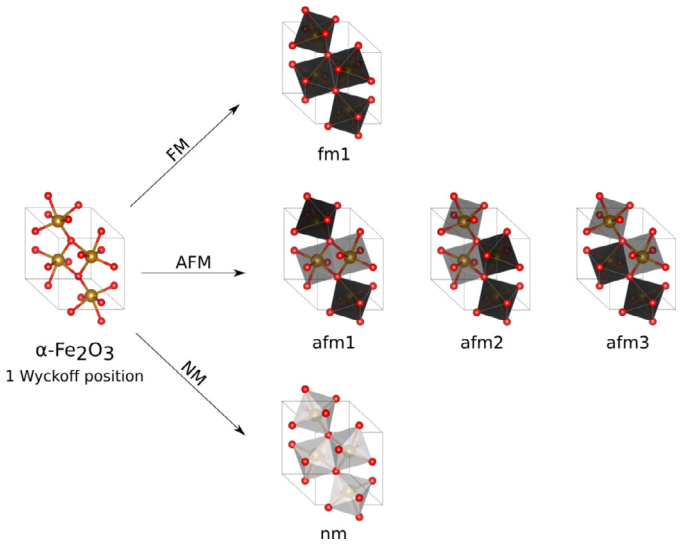

(a)

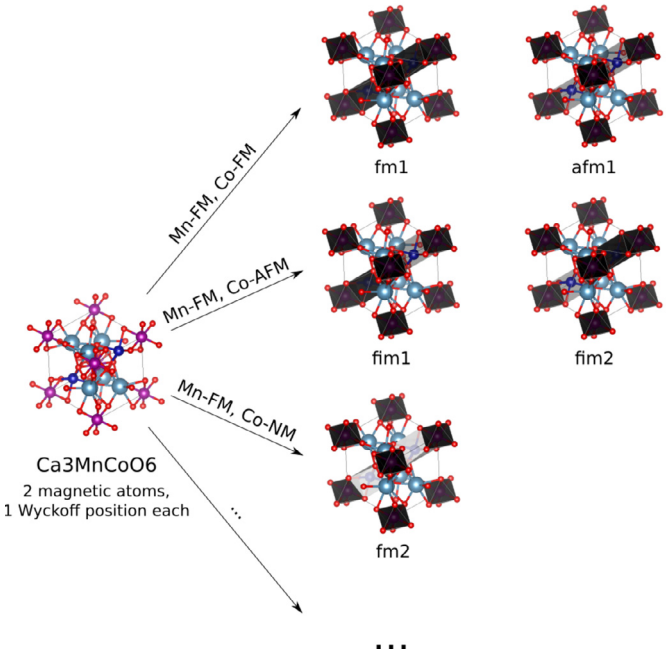

(b)

Fig. 2. Examples of trial magnetic configurations generated by Automag for our three test materials: α-Fe_2O_3 (a), Ca_3MnCoO_6 (b) and Ni_3TeO_6 (c). Black polyhedra denote spin up, grey polyhedra denote spin down and white polyhedra denote zero spin.

Given an input structure, FM, AFM and FiM configurations are generated in the following way: each Wyckoff position occupied by magnetic atoms is independently initialized in a FM, AFM or NM fashion, taking into account all possible combinations. When a Wyckoff position is initialized as AFM, enumlib [31,32] is used to generate all possible distinct splits of the atoms in this Wyckoff position into two groups to be assigned spin up and spin down states. Since it is always possible to find a new distinct split by enlarging the unit cell, the user is required to specify in input a cut-off cell size in terms of a multiple size of the input geometry. By means of this scheme, the separate initialization of different Wyckoff positions can give rise to overall FiM states. We clarify this with an example: consider the case where the magnetic atoms of a structure occupy two Wyckoff positions and consider the generated configuration where the first Wyckoff position is initialized in a FM fashion and the second in an AFM fashion. Overall, the produced magnetic state is FiM. By means of this algorithm, Automag determines the direction of magnetic moments in the trial configurations, while the absolute value of the initialized spins is user-defined and equal for all the atoms of a certain species. It is also possible for the user to give in input to Automag two absolute values for the magnetization of a single atomic species: one for high-spin (HS) states and one for low-spin (LS) states. In this case, Automag will separately initialize each Wyckoff position occupied by that atomic species with all HS or all LS states, taking into account all possible combinations. Examples of generated collinear magnetic configurations for our three test materials are shown in Fig. 2.

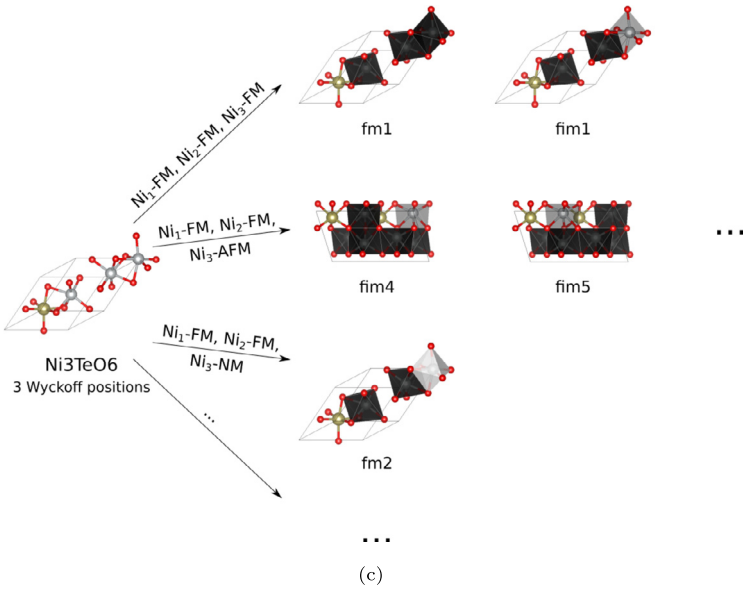

(c)

Fig. 2. (*continued*)

For the visualization of structural and magnetic data we used the software VESTA [42], which has also been used to produce Fig. 2 and all other representations of crystal structures in this paper.

The fourth step estimates the critical temperature of the magnetically ordered to paramagnetic phase transition, which is called Curie temperature in the case of FM materials and Néel temperature in the case of AFM materials. The critical temperature is obtained from a Monte Carlo simulation with the following effective Hamiltonian, which describes the magnetic interaction

$$H = H_0 - \frac{1}{2} J_1 \sum_{i \neq j} \mathbf{S}_i \cdot \mathbf{S}_j - \frac{1}{2} J_2 \sum_{i \neq j} \mathbf{S}_i \cdot \mathbf{S}_j - \frac{1}{2} J_3 \sum_{i \neq j} \mathbf{S}_i \cdot \mathbf{S}_j + \dots \quad (2)$$

where J_1 is the coupling constant assigned to first neighbors, J_2 to second neighbors, J_3 to third neighbors and so on, H_0 is a constant term which does not depend on the magnetic interaction and the $\mathbf{S}_i$ are unit vectors pointing to the positive or negative direction of the z axis, depending on the spin orientation of the corresponding magnetic atom. Since eq. (2) is rotationally invariant, the choice of the z axis is arbitrary. The first sum runs over all pairs of atoms in the unit cell which are first neighbors (for the atom j, including periodic replicas), the second sum over second neighbors and so forth. The coefficient $1/2$ in front of the coupling constants avoids the double counting for atoms i, j and j, i. The effective Hamiltonian in eq. (2) defines a three-dimensional Heisenberg model which is well-known in the literature [43], under the assumption that the $\mathbf{S}_i$ can point anywhere on the unit sphere at finite temperatures. The order parameter of this model is the normalized mean magnetization length $m(T)$, which is defined as the ensemble average of the $\mathbf{S}_i$ at a given temperature and has the following analytical form

$$m(T) = \begin{cases} \left(1 - \frac{T}{T_C}\right)^{\beta} & T \leq T_C \\ 0 & T > T_C \end{cases} \quad (3)$$

where T_C is the critical temperature and β is the critical exponent. The value of $m(T)$ against T can be obtained by taking ensemble averages with a Monte Carlo simulation and the resulting curve can be fitted with eq. (3) to obtain the values of T_C and β. For the simulation we use the VAMPIRE [27] software package, while the coupling constants J_i in eq. (2) are computed by Automag from the single-point energies of different magnetic configurations in the same cell settings. Depending on the particular system under study, we may choose to truncate the effective Hamiltonian at the first, second, third neighbors or more, in order to get a converged model. The convergence of the Heisenberg model is evaluated by computing the Pearson correlation coefficient between the DFT energies and the predicted energies of a control group of magnetic configurations. It is worth noting that this approach can be applied only if all magnetic atoms have the same absolute value of the magnetic moments.

3. Test results

We have tested the Automag code on three known antiferromagnetic materials: α-Fe_2O_3 (hematite) [38], Ca_3MnCoO_6 [39] and Ni_3TeO_6 [40]. Their experimental magnetic ground states are shown in Fig. 3 in their respective conventional cells, as found in the MAGNDATA database [44]. The magnetic ground states predicted by Automag coincide with the experimental ones for α-Fe_2O_3 and Ni_3TeCoO_6, while for Ca_3MnCoO_6 we could not compute the enthalpy of the configuration corresponding to the experimental ground state, since the initialized LS states on Co atoms turned into HS. The estimation of the Néel temperature was possible for α-Fe_2O_3 and Ni_3TeO_6 and the predicted values of 911 K and 32 K are both in good agreement with experiment (955 K and 52 K). In the case of Ca_3MnCoO_6 a model more sophisticated than eq. (2) is needed, due to the presence of two different magnetic atoms.

3.1. Convergence tests

The energy cut-off of the plane wave basis set has been checked for convergence using trial values from 500 to 1000 eV with increments of 10 eV. For the electronic smearing parameter σ trial values from 0.05 to 0.2 eV with increments of 0.05 eV have been used, while for the k-mesh resolution parameter R_k we used trial values from 20 to 100 Å with increments of 10 Å. We consider the value of a calculation parameter to be converged if it gives an error in the computed energy which is less than 1 meV/atom with respect to the most accurate energy value obtained with that parameter. When more than one value satisfies this criterion, we

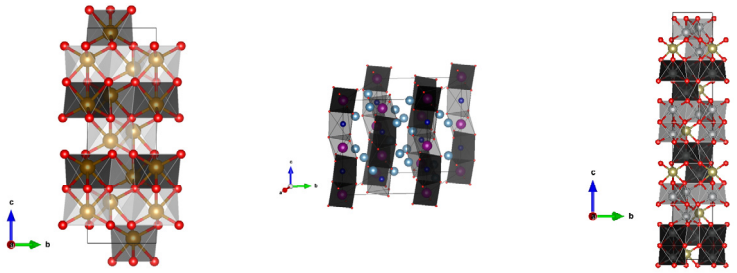

(a) α-Fe_2O_3 (b) Ca_3MnCoO_6 (c) Ni_3TeO_6

Fig. 3. The magnetic ground state of our three test materials in their respective conventional cells. Black polyhedra denote spin up and grey polyhedra denote spin down.

Table 1
Results of convergence tests for the three test materials.

	E_{cut} (eV)	σ (eV)	R_k (Å)
α-Fe_2O_3	820	0.2	20
Ca_3MnCoO_6	820	0.2	20
Ni_3TeO_6	830	0.2	20

Table 2
Calculated values of the electronic correlation parameter U by linear response for the three test materials.

Phase	Atom	U (eV)
α-Fe_2O_3	Fe	3.51
Ca_3MnCoO_6	Mn	6.64
	Co	6.76
Ni_3TeO_6	Ni	5.17

choose the least computationally expensive. Results of convergence tests for all our three test materials are reported in Table 1.

3.2. Calculation of the electronic correlation parameter U

Since all three examples are strongly correlated materials, we used the second step of Automag to calculate the linear response value of the electronic correlation parameter U for DFT+U. When studying α-Fe_2O_3 we gave in input to Automag the conventional cell, which contains six formula units, while for Ca_3MnCoO_6 and Ni_3TeO_6 we used primitive cells, which contain two and one formula units, respectively. The obtained values of U are reported in Table 2.

3.3. Search for the ground collinear magnetic state

The search for the ground collinear magnetic state of all our three test materials has been performed using their primitive cell geometry, which contains two formula units in the case of α-Fe_2O_3 and Ca_3MnCoO_6 and one formula unit in the case of Ni_3TeO_6. The cell size cut-off, instead, has been set to two formula units for all the three materials. For what concerns the absolute values of the magnetic moments, Fe atoms in α-Fe_2O_3 have been given 5 μ_B, which corresponds to the HS state of Fe^{3+}; Mn and Co atoms in Ca_3MnCoO_6 have been given 3 μ_B and 1 μ_B, respectively, which correspond to the HS state of Mn^{4+} and the LS state of Co^{2+}; Ni atoms in Ni_3TeO_6 have been given 2 μ_B, which corresponds to the HS state of Ni^{2+}. This produced 5 trial configurations in the case of α-Fe_2O_3 (shown in Fig. 2), 13 trial configurations in the case of Ca_3MnCoO_6 and 357 trial configurations in the case of Ni_3TeO_6 (both partially shown in Fig. 2). The trial set for α-Fe_2O_3 does not contain FiM configurations, since the magnetic atoms occupy only one Wyckoff position.

The ground magnetic state of α-Fe_2O_3 has been correctly identified by Automag using DFT+U with the calculation parameters

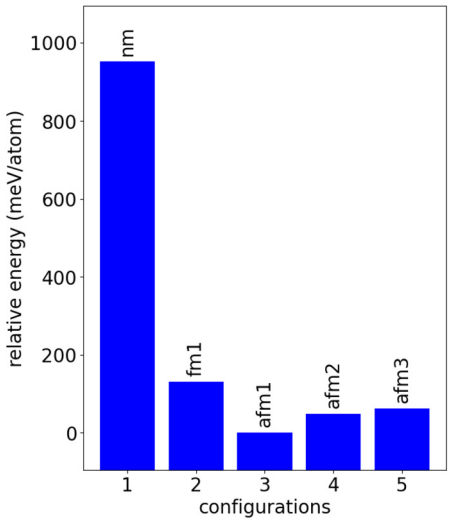

Fig. 4. The relative energies of all calculated magnetic configurations of α-Fe_2O_3. The most stable is `afm1`, which coincides with the experimental magnetic ground state.

Table 3
Initial and final values of the magnetic moments during single-point energy calculations and computed relative energies for all the trial magnetic configurations of α-Fe_2O_3.

	Conf.	Magnetic moments (μ_B)				Energy (meV/at.)
		Fe1	Fe2	Fe3	Fe4	
initial	nm	0	0	0	0	
final	nm	0	0	0	0	952.09
initial	fm1	+5	+5	+5	+5	
final	fm1	+4.306	+4.306	+4.306	+4.306	130.95
initial	afm1	+5	+5	-5	-5	
final	afm1	+4.107	+4.107	-4.107	-4.107	0.00
initial	afm2	+5	-5	+5	-5	
final	afm2	+4.170	-4.170	+4.170	-4.170	48.65
initial	afm3	+5	-5	-5	+5	
final	afm3	+4.189	-4.189	-4.189	+4.189	62.02

obtained during the previous steps of the workflow. The energy distribution of the 5 trial configurations is shown in Fig. 4, while Table 3 displays the computed energy values together with the initial and final values of the magnetic moments.

The case of Ca_3MnCoO_6 is less trivial. As shown in Table 4, for some trial configurations the magnetic moments significantly differ from their initialized values. In particular, `fm2` and `fm3` transform into something equivalent to `fim1` (recall that flipping all spins gives rise to a physically equivalent system), while `afm2` transforms into `fim5`. It is worth noting that in all configurations

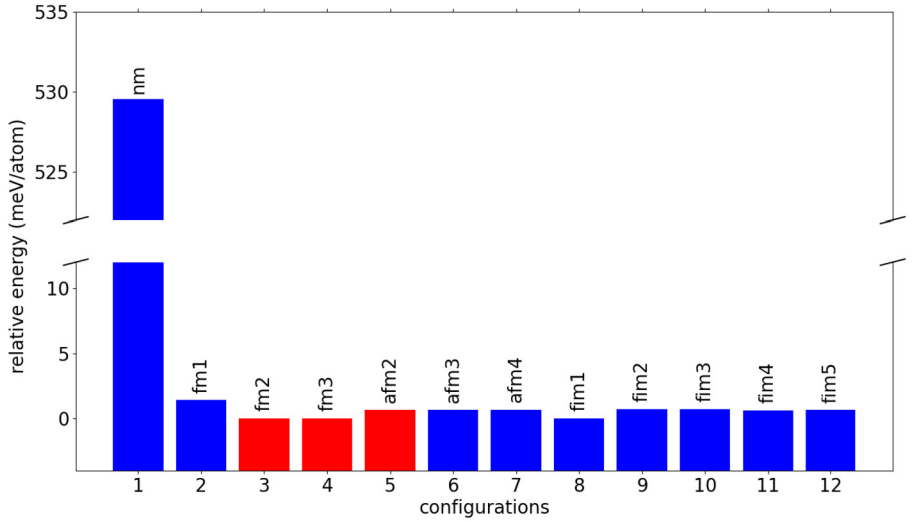

Fig. 5. Relative energies of all calculated magnetic configurations of Ca_3MnCoO_6. The most stable is `fim1`, while `afm3`, which corresponds to the experimental ground state except for the presence of HS states on Co atoms instead of LS is found at 0.65 meV/atom above. The configurations where the final magnetic moments significantly differ from their initialized values are shown in red. The configuration `afm1` is not shown, since its single-point energy does not converge after 200 electronic steps. (For interpretation of the colors in the figure(s), the reader is referred to the web version of this article.)

Table 4
Initial and final values of the magnetic moments during single-point energy calculations and computed relative energies for Ca_3MnCoO_6. The asterisk marks configurations which changed to a different one among those sampled. The energy of the `afm1` configuration did not converge after 200 electronic steps.

	Conf.	Magnetic moments (μ_B)				Energy (meV/at.)
		Mn1	Mn2	Co1	Co2	
initial	nm	0	0	0	0	
final	nm	0	0	0	0	529.53
initial	fm1	+3	+3	+1	+1	
final	fm1	+3.268	+3.268	+2.825	+2.825	1.41
initial	fm2	+3	+3	0	0	
final	fim1*	+3.271	+3.271	-2.786	-2.786	0.00
initial	fm3	0	0	+1	+1	
final	fim1*	-3.272	-3.272	+2.787	+2.787	0.01
initial	afm1	0	0	+1	-1	
final						NC
initial	afm2	+3	-3	0	0	
final	fim5*	+3.268	-3.266	-2.806	-2.806	0.65
initial	afm3	+3	-3	+1	-1	
final	afm3	+3.267	-3.267	2.807	-2.807	0.65
initial	afm4	+3	-3	-1	+1	
final	afm4	+3.267	-3.267	-2.807	+2.807	0.65
initial	fim1	+3	+3	-1	-1	
final	fim1	+3.271	+3.271	-2.786	-2.786	0.00
initial	fim2	+3	+3	+1	-1	
final	fim2	+3.271	+3.271	+2.824	-2.789	0.72
initial	fim3	+3	+3	-1	+1	
final	fim3	+3.271	+3.271	-2.789	+2.824	0.72
initial	fim4	+3	-3	+1	+1	
final	fim4	+3.266	-3.268	+2.805	+2.805	0.63
initial	fim5	+3	-3	-1	-1	
final	fim5	+3.268	-3.266	-2.806	-2.805	0.65

the magnetic moments on Co atoms turn to HS states. The calculated energies of magnetic configurations are plotted in Fig. 5. The most stable turns out to be `fim1`, while `afm3`, which corresponds to the experimental ground state [39] except for the presence of HS states on Co atoms is found at 0.65 meV/atom above `fim1`. The computed energies of the spin-polarized configurations are all identical up to numerical errors, which indicates weak magnetic coupling.

For what concerns Ni_3TeO_6, the most stable configuration turns out to be `afm79`, which coincides with the experimental ground state. Given the high number of trial configurations, Automag produces in output several histogram plots, the first of which is reported in Fig. 6. The initial and final magnetic moments, together with the computed relative energies of all configurations in Fig. 6 plus the obtained ground state are reported in Table 5. The 357 trial configurations generated by Automag have the interesting property to be written in 8 different unit cell settings, which are displayed in Fig. 7. The first settings are the same as the Ni_3TeO_6 primitive cell given in input to Automag, while the configurations containing two formula units have been written in 7 different unit cell settings, not just in a single supercell of the primitive cell. This happens because for some systems it is not possible to write all possible magnetic configurations using a single choice of the unit cell, therefore enumlib generates several of them. The first 11 configurations reported in Fig. 6 and Table 5 belong to the unit cell in Fig. 7a, while the remaining 3 belong to the unit cell in Fig. 7b. Among the 357 trial configurations, 6 (2%) did not converge after 200 electronic steps, 141 (39%) converged to a magnetic configuration which is different than the initialized one and (59%) converged to the same magnetic configuration as initialized. The similar energy of several distinct magnetic configurations signals the presence of weak coupling.

3.4. Calculation of the critical temperature

For α-Fe_2O_3 we used Automag to estimate the Néel temperature T_N of the material. Since the 4 magnetic configurations evaluated when searching for the ground magnetic state are not enough to obtain well-converged coupling constants from eq. (2), we run the collinear step again using this time the conventional cell of α-Fe_2O_3 as depicted in Fig. 3a instead of the primitive cell. This time, the initial structure contains 12 Fe atoms instead of 4 and Automag generated 92 trial configurations, all of which successfully completed single-point energy calculation without any significant change in the values of the initialized magnetic moments. We exclude the NM configuration from the computation of the critical

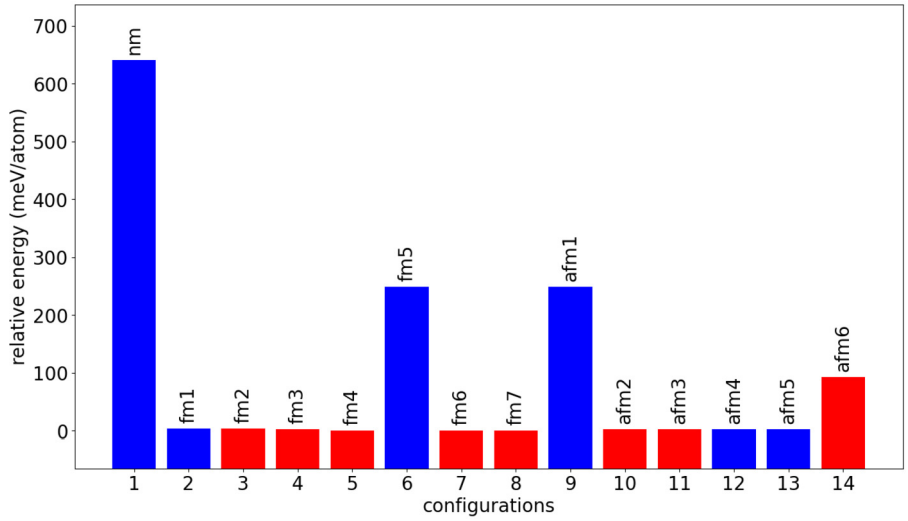

Fig. 6. Relative energies of the first 14 calculated magnetic configurations of Ni_3TeO_6. Calculations whose final magnetic moments significantly differ from their initialized values are shown in red (color online).

Table 5
Initial and final values of the magnetic moments during single-point energy calculations and computed relative energies for the first 14 configurations of Ni_3TeO_6. The obtained ground state `afm79` is also listed. The asterisk marks configurations which changed to a different one among those sampled, while the dagger marks configurations which changed to a configuration not present among those sampled.

	Conf.	Magnetic moments (μ_B)						Energy (meV/at.)
		Ni1	Ni2	Ni3	Ni4	Ni5	Ni6	
initial	nm	0	0	0				
final	nm	0	0	0				641.15
initial	fm1	+2	+2	+2				
final	fm1	+1.755	+1.770	+1.754				3.44
initial	fm2	+2	+2	0				
final	fm1*	+1.755	+1.770	+1.754				3.44
initial	fm3	+2	0	+2				
final	fim2*	+1.756	-1.764	+1.746				2.93
initial	fm4	+2	0	0				
final	fim1*	+1.736	+1.763	-1.723				0.49
initial	fm5	0	+2	+2				
final	fm5	+0.020	+1.768	+1.723				248.74
initial	fm6	0	+2	0				
final	fim1*	+1.736	+1.763	-1.723				0.49
initial	fm7	0	0	+2				
final	fim1*	-1.736	-1.763	+1.723				0.49
initial	afm1	+2	0	-2				
final	afm1	+1.737	-0.009	-1.719				248.63
initial	afm2	+2	-2	0				
final	fim2*	+1.756	-1.764	+1.746				2.93
initial	afm3	0	+2	-2				
final	fim2*	-1.756	+1.764	-1.746				2.93
initial	afm4	+2	+2	-2	-2	+2	-2	
final	afm4	+1.745	+1.745	-1.770	-1.766	+1.742	-1.735	2.07
initial	afm5	+2	+2	-2	-2	-2	+2	
final	afm5	+1.745	+1.745	-1.766	-1.770	-1.735	+1.742	2.07
initial	afm6	0	0	0	0	+2	-2	
final	fim214†	-0.003	+0.004	+0.000	-1.767	+1.733	-1.733	92.32
initial	afm79	+2	-2	-2	+2	-2	+2	
final	afm79	+1.740	-1.740	-1.757	+1.757	-1.729	+1.729	0.00

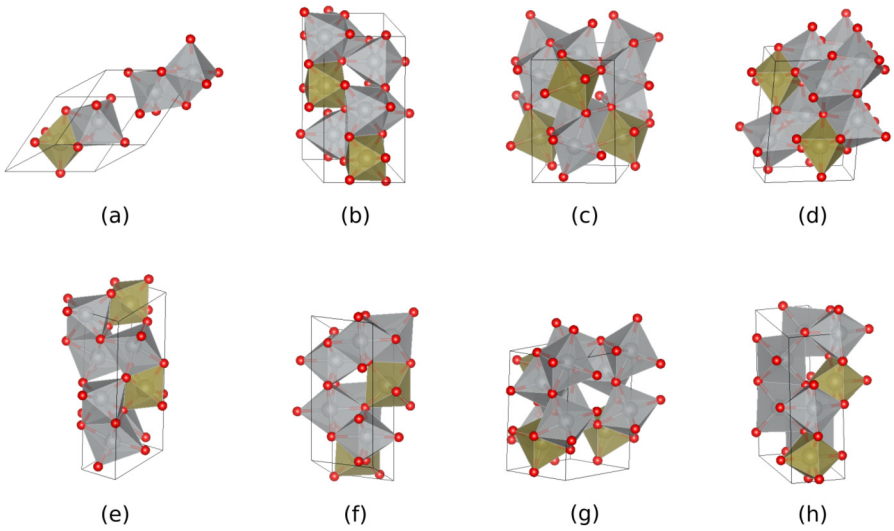

Fig. 7. Unit cell settings generated by enumlib for the 357 magnetic configurations of Ni_3TeO_6. Unit cell (a) contains one formula unit while the remaining seven contain two formula units.

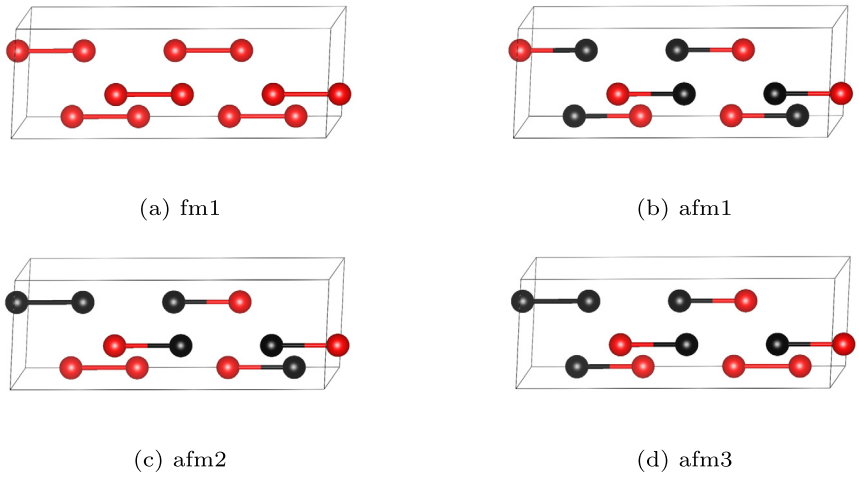

Fig. 8. The first four magnetic configurations of α-Fe_2O_3 in the conventional cell with 12 Fe atoms. Red spheres denote spin up and black spheres denote spin down (color online). For simplicity, oxygen atoms are not shown. In the unit cell, there are six pairs of Fe atoms at a distance of 2.90 Å (first neighbors). Each pair gives an energy contribution to the Heisenberg Hamiltonian equal to J_1, if the Fe atoms have equal spin, or to $-J_1$ if they have opposite spin.

temperature, since it lies outside the range of applicability of our Heisenberg Hamiltonian (we recall that the $\mathbf{S}_i$ in eq. (2) are unit vectors). This leaves us with 91 configurations. For each of them, Automag can write an equation of the form of eq. (2) in the H_0 and J_i unknowns by substituting the computed energy in H and the signs of the magnetic moments in $\mathbf{S}_i$. In other words, by using any subgroup of our 91 configurations Automag can write a system of n equations in $k+1$ unknowns, where n is the number of configurations used to fit the model and k is the number of J_i that we include in the Heisenberg Hamiltonian. For example, if we include only first neighbors, eq. (2) reads

$$H = H_0 - \frac{1}{2} J_1 \sum_{i \neq j} \mathbf{S}_i \cdot \mathbf{S}_j \tag{4}$$

In Fig. 8 we have represented the first four magnetic configurations of α-Fe_2O_3 in the conventional cell with 12 Fe atoms and we have connected with a bond the six pairs of atoms at a distance of 2.90 Å, i.e. the first neighbors. From these four configurations, substituting the $\mathbf{S}_i$, $\mathbf{S}_j$ and the H in eq. (4), we obtain the following system of equations in the H_0 and J_1 unknowns

$$\begin{cases} H_{\text{fm1}} = H_0 - 6J_1 \\ H_{\text{afm1}} = H_0 + 6J_1 \\ H_{\text{afm2}} = H_0 + 2J_1 \\ H_{\text{afm3}} = H_0 + 2J_1 \end{cases} \tag{5}$$

where H_{fm1}, H_{afm1}, H_{afm2} and H_{afm3} are the DFT energies obtained from the VASP calculations, while H_0 is a constant term which does not depend on the magnetic interaction. A similar system of equations can be written using any number of configurations and including any number of nearest neighbors. However, all the magnetic configurations used to write the system must be in the same unit cell settings, otherwise there will be no one-to-one mapping between the atoms across different settings. This is the reason why sometimes enumlib is forced to write magnetic configurations in different unit cells, in order to explore all possible combinations. The system can be solved for H_0 and J_i if the number of linearly independent equations is greater or equal than the number of unknowns. In the first case, Automag solves the system of equations to the least squares, otherwise, the exact solution is provided.

Luckily, all the 92 configurations studied using the conventional cell of α-Fe_2O_3 are written in the same unit cell settings. We use

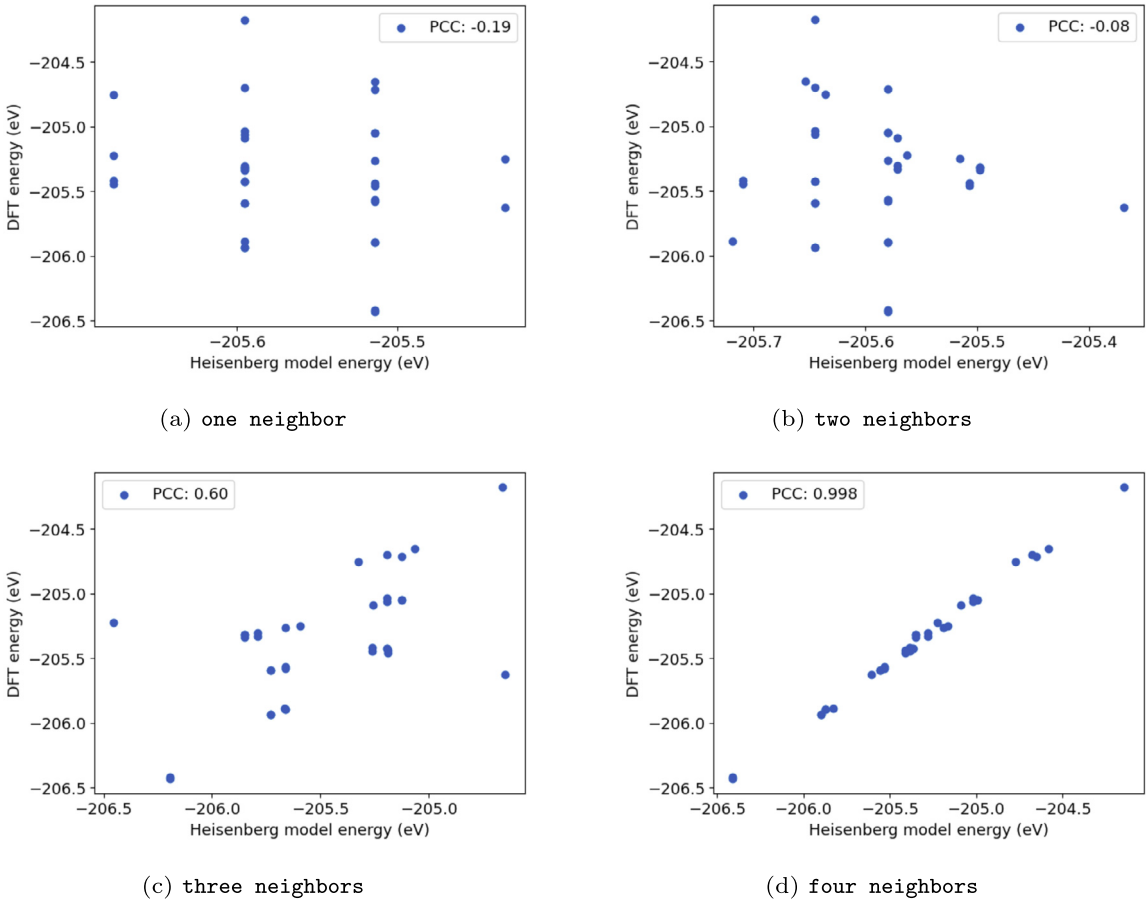

(a) `one neighbor` (b) `two neighbors`

(c) `three neighbors` (d) `four neighbors`

Fig. 9. The accuracy of the Heisemberg model which describes the magnetic interaction in α-Fe_2O_3 computed taking an increasing amount of nearest neighbors into account. With four nearest neighbors convergence is reached.

Table 6
Values of the distances between neighbors (d), counts of links in the unit cell at each distance, values of the coupling constants J_i and Pearson correlation coefficients of each Heisemberg model for α-Fe_2O_3 up to fourth nearest neighbors.

number of neighbors	d (Å)	counts	J_1	J_2	J_3	J_4	PCC
			($\times$ e-22 J/link)				
1	2.90	6	-32.61				-0.19
2	2.97	18	-25.90	+9.82			-0.08
3	3.36	18	-27.18	-8.17	-71.36		0.60
4	3.70	36	-9.79	-9.31	-71.40	-45.77	0.998

55 of them (60%) for generating the system of equations and leave aside 36 of them (40%) to form a control group. The system of equations is solved automatically, while the user needs only to choose a cut-off radius for the magnetic interaction, to determine how many nearest neighbors are taken into account, and a relative size for the control group. Once the values of H_0 and J_i have been obtained, they can be used to get the Heisenberg model energy of each configuration in the control group, which is obtained again from eq. (2), but this time by substituting the signs of the magnetic moments in the $\mathbf{S}_i$ and calculating H. The convergence of the Heisenberg model is evaluated by computing the Pearson correlation coefficient between the DFT energies and the Heisenberg model energies of all configurations in the control group and it is reported in Table 6, together with the computed values of the coupling constants. Convergence is reached by writing the Heisenberg Hamiltonian up to fourth nearest neighbors. DFT and Heisenberg model energies are plotted against each other in Fig. 9.

In output, Automag writes a unit cell file that we used for running a Monte Carlo simulation with VAMPIRE[2] for computing the ensemble averages of the mean magnetization lengths (see eq. (3)) of the spin-up and the spin-down channels, which are equal, from 0 to 1600 K at intervals of 1 K. The size of the simulation box has been set to 5x5x5 nm and Monte Carlo averages have been computed over 40.000 time steps after 20.000 equilibration steps. The obtained curve has been fitted with eq. (3), obtaining a Néel temperature $T_N = 911$ K and a critical exponent $\beta = 0.34$. This last value is in excellent agreement with the theoretical solution of the Heisenberg model, which gives $\beta = 0.33$ as a universal constant for 3D materials. The mean magnetization length of the spin-up channel obtained from the Monte Carlo simulation and its analytical fit are plotted in Fig. 10. The computed value of the Néel temperature for α-Fe_2O_3 is very close to the experimental value of 955 K [38].

For Ca_3MnCoO_6, we could not use eq. (2) to model the magnetic interaction since there are two types of magnetic atoms (Mn and Co). For being able to treat such cases, an extension of the Heisenberg model in eq. (2) is needed, and this is currently not implemented in the VAMPIRE code.

For Ni_3TeO_6, we tried to estimate the Néel temperature using the 49 magnetic configurations in the unit cell settings reported in Fig. 7e, generated during the search for the ground magnetic state. These are the settings in which the magnetic ground state `afm79` is written. For 1 configuration (2%) the single-point energy

[2] VAMPIRE software package version 5.0 (Version c0cb858d7dcdcdfc647493-8324e363599e728b30) available from https://vampire.york.ac.uk.

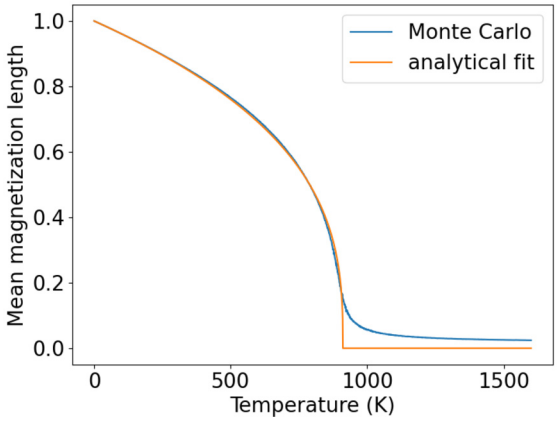

Fig. 10. Mean magnetization length of the spin-up channel with respect to temperature for the effective Hamiltonian describing the magnetic interaction in α-Fe_2O_3 written up to fourth nearest neighbors. The Néel temperature and the critical exponent calculated from a least squares fit are T_N = 911 K and $\beta = 0.34$.

did not converge after 200 electronic steps, while for 19 configurations (39%) the final values of the magnetic moments significantly differ from the initial ones. In addition, 1 of the remaining configurations contains Ni atoms in the NM state, which is outside the range of applicability of our Heisenberg Hamiltonian (we recall that the $\mathbf{S}_i$ in eq. (2) are unit vectors), therefore it cannot be used to fit the model. This leaves 28 configurations (57%) available to obtain coupling constants from eq. (2) and to form a control group for evaluating the accuracy of the Heisenberg model. Again, we choose a relative size of the control group of 40%, which means that 17 configurations form the fit group and 11 configurations form the control group. The most accurate coupling constants, corresponding to a PCC value of 0.97, are obtained by including in eq. (2) magnetic interactions up to fifth nearest neighbors. The DFT and the Heisenberg model energies of the 11 configurations in the control group are plotted against each other in Fig. 11a, while the obtained values of the coupling constants are reported in Table 7. The values of the distances between neighbors and the counts of all pairs of Ni atoms in the unit cell at each distance are reported in Table 8 up to sixth nearest neighbors. Unfortunately, the obtained Heisenberg model is not sufficiently well-converged for our purposes and cannot be used to estimate the Néel temperature of `afm79`, since, according to the Heisenberg model energies, the configuration `fim1` is erroneously predicted to be the ground state of the system, while the experimental ground state `afm79`,

Table 7
Values of the coupling constants J_i and Pearson correlation coefficients of two Heisemberg models for Ni_3TeO_6. The first has been fitted using 17 configurations in the unit cell settings reported in Fig. 7e, which has stoichiometry $Ni_6Te_2O_{12}$, and it does not reproduce the correct magnetic ground state. The second has been fitted using 78 configurations in a 1x2x1 supercell of the previous unit cell, it correctly reproduces the magnetic ground state and it has been used to estimate the Néel temperature of the material.

number of neighbors	J_1	J_2	J_3	J_4	J_5	J_6	PCC
	($\times$ e-22 J/link)						
5	3.22	1.35	-3.22	-1.60	-5.34		0.97
6	3.15	1.54	-2.97	-1.43	-5.23	-2.04	0.99

Table 8
Values of the distances between neighbors (d) and counts of links in the unit cell at each distance for Ni_3TeO_6, up to sixth nearest neighbors.

number of neighbors	d (Å)	counts
1	2.78	4
2	3.00	12
3	3.46	12
4	3.68	12
5	3.79	12
6	4.02	4

correctly predicted by DFT, lies 0.20 meV/atom above `fim1` according to the Heisenberg model. If we try to improve the model by including more neighbors, the resulting system of equations becomes singular.

In order to increase the number of available configurations to fit the Heisenberg model, we run the collinear step of Automag one more time, using a 1x2x1 supercell of the unit cell in Fig. 7e. This time, Automag generated 248 magnetic configurations, 1 of which (0.4%) reported an error during single-point energy calculation. In addition, for 23 configurations (9.3%) the single-point energy did not converge after 200 electronic steps and for 92 configurations (37.1%) the final values of the magnetic moments significantly differ from the initial ones. Similarly to the previous case, 2 of the remaining configurations cannot be used to fit the Heisenberg model because they contain Ni atoms in the NM state, leaving a pool of 130 configurations (52.4%) available to fit the model and to evaluate its accuracy. With a relative size of the control group of 40%, we get 78 configurations in the fit group and 52 in the control group. This time, we have enough configurations to fit a model which takes into account magnetic interactions up to sixth nearest neighbors. The obtained Heisenberg model, with a PCC of 0.99,

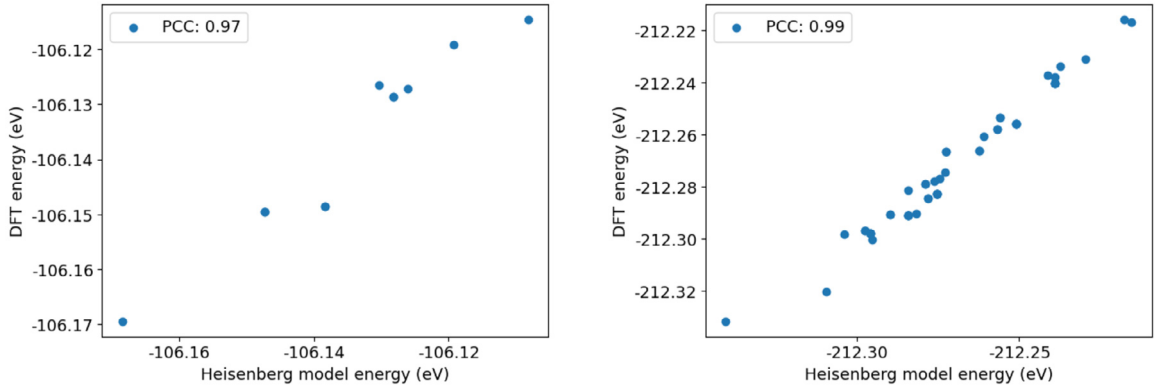

(a) five neighbors (b) six neighbors

Fig. 11. The accuracy of two Heisemberg models which describe the magnetic interaction in Ni_3TeO_6 computed (a) taking into account magnetic interactions up to fifth nearest neighbors in the unit cell settings reported in Fig. 7e and (b) taking into account magnetic interactions up to sixth nearest neighbors in a 1x2x1 supercell of the previous unit cell.

Table 9
Energies of the three most stable configurations according to DFT and to our Heisenberg model obtained taking into account the magnetic interaction up to sixth nearest neighbors. Notice that Heisenberg model energies are closer than DFT energies.

configuration	E_{DFT} (meV/at.)	E_H (meV/at.)
afm61	0.00	0.00
afm119	0.20	0.06
fim1	0.51	0.11

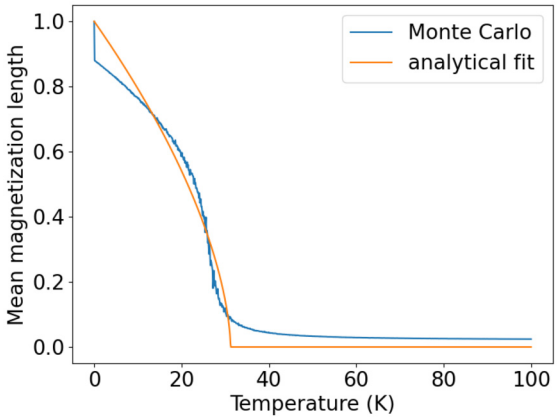

Fig. 12. Mean magnetization length of the spin-up channel with respect to temperature for the effective Hamiltonian describing the magnetic interaction in Ni_3TeO_6 written up to sixth nearest neighbors. The Néel temperature and the critical exponent calculated from a least squares fit are T_N = 31 K and $\beta = 0.60$.

is more accurate than the previous and it correctly reproduces the magnetic ground state of the system, now denoted as `afm61`. However, the energy differences between the ground state and the lowest-energy metastable configurations given by the Heisenberg model are smaller if compared to DFT results (see Table 9). The DFT and the Heisenberg model energies of the 52 configurations in the control group are plotted in Fig. 11b, while the obtained values of the coupling constants are reported in Table 7. If we try to include more neighbors in the Heisenberg Hamiltonian, the resulting system of equations becomes singular.

We used our most accurate Heisenberg model to run a Monte Carlo simulation with the VAMPIRE software package, in order to estimate the Néel temperature of Ni_3TeO_6. We computed the ensemble averages of the mean magnetization lengths of the spin-up and the spin-down channels from 0 to 100 K at intervals of 0.1 K. The size of the simulation box has been set to 5x5x5 nm and Monte Carlo averages have been computed over 40.000 time steps after 20.000 equilibration steps. The obtained curve has been fitted to the least squares with eq. (3), obtaining a Néel temperature $T_N = 31$ K and a critical exponent $\beta = 0.60$. The estimated critical temperature is not far from the experimental value (52 K), while the anomalously high value of the critical exponent can be explained by the mixing of the almost isoenergetic configurations reported in Table 9, which dampens the magnetization curve (see Fig. 12).

4. Conclusions

We have presented the Automag code and we have reported the results of tests on α-Fe_2O_3, Ca_3MnCoO_6 and Ni_3TeO_6, all well-known collinear antiferromagnetic materials. These results are very promising, since both the predicted magnetic ground states and the estimated values of the Néel temperatures are in good agreement with experiment. This happens despite the test materials having non-trivial nuances, such as the presence of two magnetic atomic species in the case of Ca_3MnCoO_6 and the presence of Ni atoms in three different Wyckoff positions in the case of Ni_3TeO_6. This makes us confident that Automag can be successfully used to predict the magnetic ground state of unknown materials. At the moment, only collinear magnetic configurations are considered, so if the material exhibits non-collinear magnetism, Automag can find only a collinear approximation of the magnetic ground state. In the future, we plan to extend Automag to treat also non-collinear magnetism. In addition, it is worth noting that the current way of generating magnetic configurations may lead to a huge combinatorial space for big unit cell cut-offs. In order to avoid this problem, in the future we plan to limit the splitting of Wyckoff positions to those which break the original symmetry of the parent structure only up to a certain user-defined degree, using group-subgroup relations. Finally, we notice that Automag with minor modification could also be used for predicting lowest energy atomic ordering in alloys and, just like for magnetism, producing a complete set of configurations that can then be used to fit an effective Hamiltonian and perform studies (by Monte Carlo) of order-disorder transitions, configurational entropies and stability of solid solutions.

Declaration of competing interest

The authors declare that they have no known competing financial interests or personal relationships that could have appeared to influence the work reported in this paper.

Data availability

The corresponding author has shared the link to the Automag code with the journal and has reported it in the present article.

Acknowledgements

We acknowledge the Ministry of Science and Higher Education agreement No. 075-15-2020-808.

Appendix A. Supplementary material

Supplementary material related to this article can be found online at https://doi.org/10.1016/j.cpc.2022.108571.

References

[1] A.R. Oganov, C.J. Pickard, Q. Zhu, R.J. Needs, Nat. Rev. Mater. 4 (2019) 331.
[2] A. Gavezzotti, Acc. Chem. Res. 27 (1994) 309.
[3] P. Ball, Nature 381 (1996) 648.
[4] P. Hohenberg, W. Kohn, Phys. Rev. 136 (1964) B864.
[5] W. Kohn, L.J. Sham, Phys. Rev. 140 (1965) A1133.
[6] T.S. Bush, C.R.A. Catlow, P.D. Battle, J. Mater. Chem. 5 (1995) 1269.
[7] S.M. Woodley, P.D. Battle, J.D. Gale, C.R.A. Catlow, Phys. Chem. Chem. Phys. 1 (1999) 2535.
[8] S.M. Woodley, in: Applications of Evolutionary Computation in Chemistry, Springer, 2004, pp. 95–132.
[9] D.M. Deaven, K.-M. Ho, Phys. Rev. Lett. 75 (1995) 288.
[10] A.R. Oganov, C.W. Glass, J. Chem. Phys. 124 (2006) 244704.
[11] A.O. Lyakhov, A.R. Oganov, M. Valle, Comput. Phys. Commun. 181 (2010) 1623.
[12] A.O. Lyakhov, A.R. Oganov, H.T. Stokes, Q. Zhu, Comput. Phys. Commun. 184 (2013) 1172.
[13] R. Martoňák, A. Laio, M. Parrinello, Phys. Rev. Lett. 90 (2003) 075503.
[14] R. Martoňák, et al., Z. Kristallogr. 220 (2005) 489.
[15] S. Goedecker, J. Chem. Phys. 120 (2004) 9911.
[16] Y. Wang, J. Lv, L. Zhu, Y. Ma, Phys. Rev. B 82 (2010) 094116.
[17] M.U. Schmidt, U. Englert, J. Chem. Soc., Dalton Trans. (1996) 2077.
[18] C.J. Pickard, R.J. Needs, Phys. Rev. Lett. 97 (2006) 045504.
[19] J. Pannetier, J. Bassas-Alsina, J. Rodriguez-Carvajal, V. Caignaert, Nature 346 (1990) 343.
[20] J.C. Schön, M. Jansen, Angew. Chem., Int. Ed. Engl. 35 (1996) 1286.
[21] J.P. Perdew, K. Burke, M. Ernzerhof, Phys. Rev. Lett. 77 (1996) 3865.
[22] G. Kresse, D. Joubert, Phys. Rev. B 59 (1999) 1758.
[23] G. Kresse, J. Hafner, Phys. Rev. B 47 (1993) 558.
[24] G. Kresse, J. Hafner, Phys. Rev. B 49 (1994) 14251.

[25] G. Kresse, J. Furthmüller, Phys. Rev. B 54 (1996) 11169.
[26] A. Jain, et al., Concurr. Comput., Pract. Exp. 27 (2015) 5037.
[27] R.F.L. Evans, et al., J. Phys. Condens. Matter 26 (2014) 103202.
[28] M.K. Horton, J.H. Montoya, M. Liu, K.A. Persson, npj Comput. Mater. 5 (2019) 1.
[29] K. Mathew, et al., Comput. Mater. Sci. 139 (2017) 140.
[30] S.P. Ong, et al., Comput. Mater. Sci. 68 (2013) 314.
[31] G.L.W. Hart, R.W. Forcade, Phys. Rev. B 77 (2008) 224115.
[32] G.L.W. Hart, L.J. Nelson, R.W. Forcade, Comput. Mater. Sci. 59 (2012) 101.
[33] M. Cococcioni, S. De Gironcoli, Phys. Rev. B 71 (2005) 035105.
[34] V.I. Anisimov, J. Zaanen, O.K. Andersen, Phys. Rev. B 44 (1991) 943.
[35] V.I. Anisimov, I.V. Solovyev, M.A. Korotin, M.T. Czyżyk, G.A. Sawatzky, Phys. Rev. B 48 (1993) 16929.
[36] I.V. Solovyev, P.H. Dederichs, V.I. Anisimov, Phys. Rev. B 50 (1994) 16861.
[37] A. Jain, et al., APL Mater. 1 (2013) 011002.
[38] A.H. Hill, et al., Chem. Mater. 20 (2008) 4891.
[39] Y.J. Choi, et al., Phys. Rev. Lett. 100 (2008) 047601.
[40] I. Živković, K. Prša, O. Zaharko, H. Berger, J. Phys. Condens. Matter 22 (2010) 056002.
[41] S.L. Dudarev, G.A. Botton, S.Y. Savrasov, C.J. Humphreys, A.P. Sutton, Phys. Rev. B 57 (1998) 1505.
[42] K. Momma, F. Izumi, J. Appl. Crystallogr. 44 (2011) 1272.
[43] M. Plischke, B. Bergersen, Equilibrium statistical physics, World scientific, 1994.
[44] S.V. Gallego, et al., J. Appl. Crystallogr. 49 (2016) 1750.